DC Fault Characteristics of Battery Energy Storage System Based on Different Grid-Connected Structures

Qingyao Sun[1], Weijie Wen[1], Huiwen He[2], Lei Wang[2], Jiangang Xu[3], Yang Xu[4], Bin Li[1])*

[1]*Key Laboratory of Smart Grid of Ministry of Education, Tianjin University, Tianjin, China.*
[2]*China Electric Power Research Institute, Wuhan, China*
[3]*State Grid Jiangsu Electric Power Co., Ltd., Nanjing, China*
[4]*State Grid Jiangsu Electric Power Co., Ltd. Research Institute, Nanjing, China*
**weijie.wen@tju.edu.cn*

Keywords: BATTERY ENERGY STORAGE SYSTEM, FAULT ANALYSIS, DC/DC CONVERTERS

Abstract

To optimize the protection scheme of battery energy storage systems (BESSs) in the future, characteristics of DC fault current of BESSs with different grid-connected structures are studied in this paper. During the research, three grid-connected structures for BESS are analyzed, including battery clusters connected directly (structure_1), battery clusters connected through non-isolated DC/DC converter (structure_2), battery clusters connected through isolated DC/DC converter (structure_3). The equivalent circuit and the numerical calculation method of fault current are provided. The theoretical analysis is verified by simulation in PSCAD/EMTDC. The research results proved that the fault current has high peak value and rapid rise speed when non-isolated DC/DC is used, which poses great technical challenges to protective devices, such as fuse and DC breaker. Finally, comparison of three grid-connected structures is conducted. Only if DC breaker technology for BESS is broken through, battery clusters connected through non-isolated DC/DC converter is both cost-effective and high-efficient, making it more suitable for integration into large-scale BESS systems.

1 Introduction

Battery Energy Storage System (BESS) is a type of energy storage system that stores electrical energy in batteries in the form of chemical energy, which can store and release energy flexibly during the charging and discharging processes of the battery. With advantages of high energy density, large capacity, good dynamic response capability, and strong flexibility, BESS can satisfy the requirements of large-capacity energy storage facilities in the future [1].

During periods of low electricity demand in the grid, BESS can be controlled to be an active load for the main distribution grid, and during periods of high electricity demand in the grid, BESS can be controlled to be a source for the main distribution. In this way, BESS can be used to relieve the significant peak-to-valley pressure faced by the current power supply, reducing energy wastage and installed capacity requirements, minimizing line losses, and saving investment costs.

The typical structure of BESS is shown in Fig.1(a), which mainly consists of battery system, power conversion system (PCS), and battery management system (BMS) [2]. Battery system is the primary component of the BESS and can operate in two modes: charging mode and discharging mode. As shown in Fig.1(b), battery system can be divided into three levels: battery cells, battery modules, and battery clusters. Multiple battery cells are connected in series or parallel to form a battery module, and multiple battery modules are connected in series or parallel to form a battery cluster. PCS is used to facilitate the energy exchange between battery system and the grid [3]. Battery cluster serves as the basic output unit for grid connection, with DC voltage transformed through PCS and connected to the main AC grid. The configuration of PCS represents the grid-connected structure of the battery system. BMS collects information from various devices within BESS to ensure the safe operation of batteries [4].

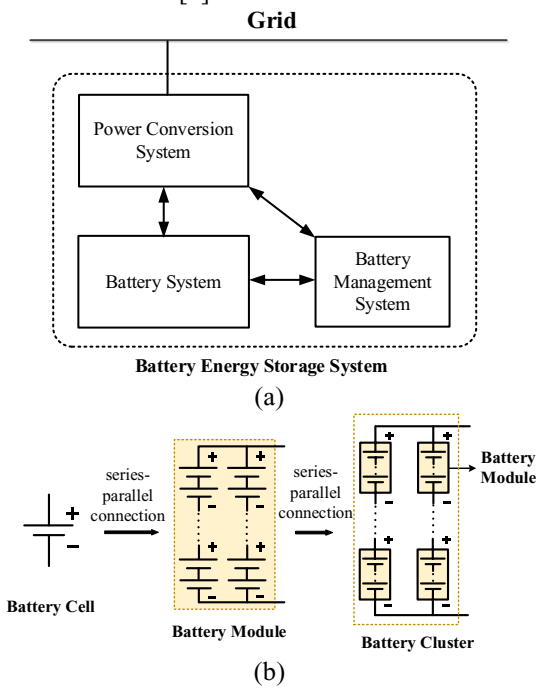

Fig. 1 Structure of battery energy storage system. (a)overall composition, (b) structure of battery system.

https://doi.org/10.1049/icp.2024.2264

The grid-connected structures of battery clusters impact the DC fault characteristics of DC line faults in BESS significantly. Existing research mainly focuses on the study of short-circuit faults between individual battery cells within the battery system [5-6], lacking analysis of the characteristics of DC line faults in BESS under different grid-connected structures.

To fulfill the research gap, the DC line fault characteristics and requirements for current interruption of BESS are demonstrated in this paper based on different grid-connected structures. In Section 2, three basic grid-connected structures of BESS are primarily introduced. In Section 3, for each grid-connected structure, equivalent circuit and the numerical calculation method for pole-to-pole faults are proposed, theoretical analysis results are validated through PSCAD simulation. In Section 4, a comparison of the three grid-connected structures is presented.

2 Brief of grid-connected structures for BESS

In order to accurately clarify the characteristics of DC faults under various grid-connected structures of BESS and further refine the protection schemes for BESS, it is necessary to conduct detailed analysis based on different grid-connected structures. Three basic grid-connected structures are introduced as follow.

2.1 Battery clusters connected directly (structure_1)

The topology of structure_1 is shown in Fig.2(a), where each battery cluster is directly connected to DC/AC converter in parallel, and increasing the number of parallel battery clusters can enhance the capacity of BESS. This grid-connected structure utilizes only DC/AC converter for energy conversion, requiring fewer power semiconductors and resulting in higher energy conversion efficiency. Under structure_1, in order to match the DC side voltage with the AC side voltage, a large number of battery cells need to be connected in series within each battery cluster to output a higher voltage level. However, due to differences in individual cell parameters and operating temperatures, actual output power imbalances and circulating currents may occur between different clusters. This circulating current leads to a gradual amplification of cluster-to-cluster differences over time and affects the internal state of each cluster within the entire battery system, increasing the difficulty of power balance control. Hence, resolving these issues is essential in practical applications to enhance the operational efficiency of BESS.

2.2 Battery clusters connected through non-isolated DC/DC converter (structure_2)

The topology of structure_2 is shown in Fig.2(b). The battery clusters are boosted by non-isolated DC/DC converters, and then the power exchange with the AC grid is carried out through DC/AC converters. A DC/DC converter is installed at the front end of each battery cluster to regulate the output voltage and achieve balanced power distribution among the clusters, thereby eliminating imbalance caused by individual differences and effectively suppressing circulating currents. Non-isolated bidirectional DC/DC converters are typically implemented using the Buck-Boost circuit. The Buck-Boost converter features a simple structure, low control complexity, good economy, and high conversion efficiency. However, it lacks electrical isolation function and may lead to interference issues between devices, which is detrimental to the safe and reliable operation of the system.

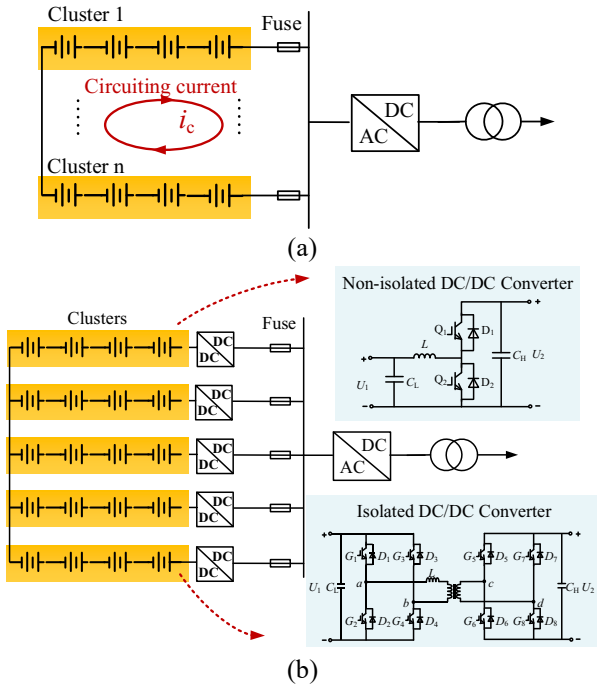

Fig. 2 Three grid-connected structures for BESS. (a) structure_1, (b) structure_2 and structure_3.

2.3 Battery clusters connected through isolated DC/DC converter (structure_3)

The topology of structure_3 is shown in Fig.2(b). The difference between structure_2 and structure_3 lies in the DC/DC converter structures: Structure_3 uses isolated DC/DC converters for energy conversion, while structure_2 employs non-isolated DC/DC converters. DAB is a typical isolated DC/DC converter, which utilizes a high-frequency transformer to achieve electrical isolation, ensuring the safe and reliable operation between the grid and the battery system. By isolating the battery cluster from the DC bus, it prevents the flow of current from the battery cluster to the opposite side of DAB, effectively eliminating potential circulating current issues among clusters. However, this approach has some drawbacks, mainly including a complex structure, higher costs, and the need for multiple sets of isolation drive circuits. Additionally, due to the bidirectional energy transfer requiring the use of high-frequency transformers, this results in reduced efficiency and increased costs.

Both structure_2 and structure_3 achieve inter-cluster balance control by installing DC/DC converters at the front end of the battery clusters, resolving circulating current issues among different clusters that are present in structure_1. Furthermore, by adjusting the DC/DC converter, the output

voltage of battery clusters can be matched with the DC side voltage of the DC/AC converter, reducing the voltage level of the battery clusters and thus reducing the difficulty for balancing and monitoring in BMS.

3 Fault analysis for different grid-connected structures

3.1 Numerical calculation method of fault current

To simplify the analysis, a battery cluster is equivalent to an electrochemical model of a single battery in this paper. As shown in Fig.2, the improved Shepherd battery model consists of a controllable voltage source and a constant resistor (r) connected in series. The internal electromotive force (E) and the output voltage of the battery model (v_{batt}) can be represented as (1) and (2) respectively. Here, E_0 is the constant voltage of the battery, K is the polarization voltage, Q is the battery capacity, SOC is the state of charge, and A and B are the exponential term coefficients. i_{batt} is the output current of the battery.

$$\begin{cases} E = E_0 - K \cdot \dfrac{1}{SOC} + A \cdot e^{-B \cdot Q \cdot (1-SOC)} \\ SOC = \dfrac{Q - \int i_{batt} dt}{Q} \end{cases} \tag{1}$$

$$v_{batt} = E - i_{batt} r \tag{2}$$

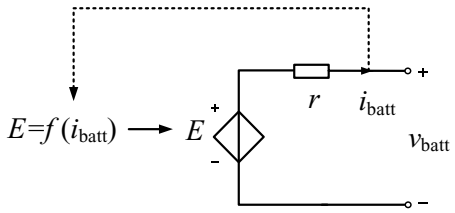

Fig. 3 Schematic diagram of the battery model.

In the event of a fault in DC line of a BESS, pole-to-pole faults are the most serious, which have a significant impact on the overall stability of the system. Therefore, the following analysis is primarily focused on pole-to-pole faults and assumes that the battery cluster is in discharging mode.

3.1.1 Fault analysis of BESS with structure_1

In structure_1, multiple battery clusters are connected in parallel first and then collectively integrated into the DC bus. When a pole-to-pole fault occurs on the DC line connected at both ends of the battery cluster, the fault equivalent circuit is shown in Fig.3. Assuming the equivalent resistance and inductance of the line between the battery cluster and the fault point are R_l and L_l, and the short-circuit resistance is R_f.

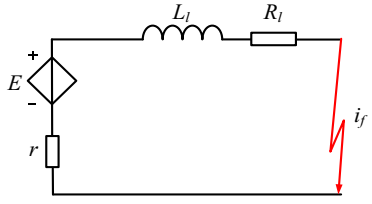

Fig. 4 Fault equivalent circuit in structure_1.

The discharge loop is directly formed between the battery and the fault point. Based on Fig.3, the fault loop equation with fault current (i_f) as a state variable can be expressed as (3). (3) is a first-order dynamic circuit, where $R = R_l + R_f$.

$$L_l \frac{di_f}{dt} + (R + r) i_f = E \tag{3}$$

Assuming the initial time of the fault, the current on the DC line is I_0. By solving (3), the expression for i_f can be obtained as (4). From (4), it is known that the fault current rises very quickly.

$$i_f = I_0 e^{-\frac{R+r}{L_l} t} + \frac{E}{R + r} \tag{4}$$

After the transient component decays, the circuit reaches a steady state, and i_f is only determined by the internal characteristics of the battery and the fault distance.

3.1.2 Fault analysis of BESS with structure_2

In structure_2, a battery cluster is connected to the DC bus through a Buck-Boost converter. When the battery cluster is in discharging mode, Q_1 is in off-state, and Q_2 is in on-state, and the direction of inductor current (i_L) is shown in Fig.5. After a pole-to-pole fault on the DC line on the high-voltage side of the Buck-Boost converter, the fault equivalent circuit is shown in Fig.5. At the moment of fault occurrence, Q_2 immediately turns off to self-protection. Based on the fault characteristics after the fault occurs, the development of fault mainly goes through two stages [7-8].

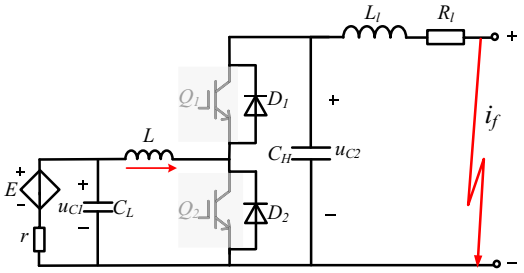

Fig. 5 Schematic diagram of equivalent circuit in structure_2.

Stage 1: the C_H discharge stage. The fault circuit is shown in Fig.5, where D_1 conducts, and D_2 withstands reverse voltage at both ends to remain off-state.

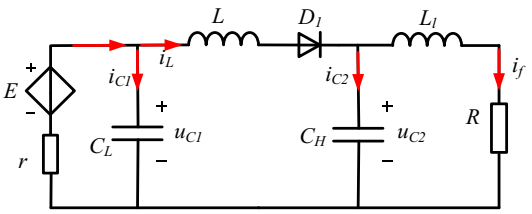

Fig. 6 Fault equivalent circuit of stage 1 in structure_2.

According to the fault circuit, the expression for the fault circuit in this stage can be obtained as (5), with low-voltage side voltage of Buck-Boost converter (u_{C1}), high-voltage side voltage (u_{C2}), i_L and i_f as state variables, Assuming the initial values of the state variables as $i_f(0) = 0$, $i_L(0) = I_{L0}$, $u_{C1}(0) = U_{C10}$, $u_{C2}(0) = U_{dc}$.

$$\begin{bmatrix} \frac{du_{C1}}{dt} \\ \frac{du_{C2}}{dt} \\ \frac{di_L}{dt} \\ \frac{di_f}{dt} \end{bmatrix} = \begin{bmatrix} -\frac{1}{rC_L} & 0 & -\frac{1}{C_L} & 0 \\ 0 & 0 & \frac{1}{C_H} & -\frac{1}{C_H} \\ \frac{1}{L} & -\frac{1}{L} & 0 & 0 \\ 0 & \frac{1}{L_l} & 0 & -\frac{R}{L_l} \end{bmatrix} \begin{bmatrix} u_{C1} \\ u_{C2} \\ i_L \\ i_f \end{bmatrix} + \begin{bmatrix} \frac{1}{rC_L} \\ 0 \\ 0 \\ 0 \end{bmatrix} E \quad (5)$$

According to (5), the fault current in this stage is solely provided by C_H. The discharge circuit of C_H forms a first order zero-input circuit, causing i_f to rise rapidly. Due to the presence of L, i_L cannot undergo a sudden change. The battery cluster and C_L charge towards C_H, but at a much slower rate compared to the discharge rate of C_H, resulting in a rapid decrease in u_{C2}.

Stage 2: the stage of all diodes conduction. At $t = t_1$, C_H is fully discharged, entering the phase of full conduction of the diodes. Both D_1 and D_2 conduct simultaneously, clamping u_{C2} to 0. Assuming the initial values for the state variables in this stage are $i_f(t_1) = I_1$, $i_L(t_1) = I_{L1}$, $u_{C1}(t_1) = U_{C1}$, $u_{C2}(t_1) = 0$. Because $u_{C2}(0) = 0$, the circuit can be decomposed into two parts as shown in Fig.7 for separate analysis. It is worth noting that the direction of i_L is opposite to the forward conduction direction of D_2 in Fig.7(a), for the sake of analysis. The total current flowing through D_2 (i_{D2}) is given by (6), and still complies with its unidirectional conduction characteristic.

$$i_{D2}(t) = i_f(t) - i_L(t) \quad (6)$$

According to the fault circuit diagram in Fig.7(b), the freewheeling diode circuit forms a first-order zero-input circuit, and the expression for the fault current is given by (7). Based on the fault circuit diagram in Fig.7(a), the discharge circuit of the low-voltage side forms a second-order circuit, and the fault circuit equation with i_L as state variable is shown in (8).

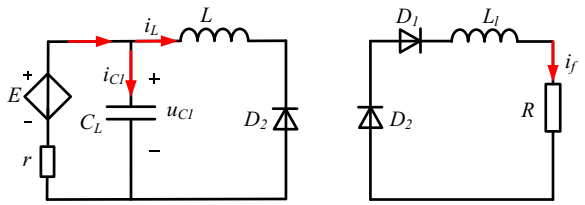

Fig. 7 Fault equivalent circuit of stage 2 in structure_2. (a) the discharge circuit of the low-voltage side, (b) the freewheeling diode circuit.

$$i_f(t) = I_1 e^{-\frac{R}{L_l}(t-t_1)} \quad (7)$$

$$rLC_L \frac{d^2 i_L}{dt^2} + L\frac{di_L}{dt} + ri_L = E \quad (8)$$

The state equation for this stage can be derived from (7) and (8) as:

$$\begin{bmatrix} \frac{du_{C1}}{dt} \\ \frac{du_{C2}}{dt} \\ \frac{di_L}{dt} \\ \frac{di_f}{dt} \end{bmatrix} = \begin{bmatrix} -\frac{1}{rC_L} & 0 & -\frac{1}{C_L} & 0 \\ 0 & 0 & 0 & 0 \\ \frac{1}{L} & 0 & 0 & 0 \\ 0 & 0 & 0 & -\frac{R}{L_l} \end{bmatrix} \begin{bmatrix} u_{C1} \\ u_{C2} \\ i_L \\ i_f \end{bmatrix} + \begin{bmatrix} \frac{1}{rC_L} \\ 0 \\ 0 \\ 0 \end{bmatrix} E \quad (9)$$

After i_{D2} decreases to zero, D_2 is turned off again, and C_H undergoes charging and discharging, bringing the fault back to stage 1. After a certain period, the system progresses to stage 2, continuing in this cycle. When the system reaches a steady state, C_H stops charging and discharging, and only the battery cluster continues to supply current to the fault point. The steady-state fault current depends on the battery discharge status. As the discharge time increases, the state of charge (SOC) gradually decreases, and the fault current also decreases. This process typically lasts for several hours.

3.1.3 Fault analysis of BESS with structure_3

In structure_3, the battery cluster is connected to the DC bus through the DAB converter. Under normal conditions, the direction of energy flow on the DAB converter is shown in Fig.8(a). When a pole-to-pole fault occurs on the output side DC line of the DAB converter, the equivalent circuit is shown in Fig.8(b).

After the fault occurs, IGBTs in the two H-bridges immediately shut down. The DAB has electrical isolation, battery cluster cannot supply current to the fault point. Therefore, the fault development process can be divided into two stages as shown in Fig.8(b): the capacitor discharge stage and the diode conduction stage.

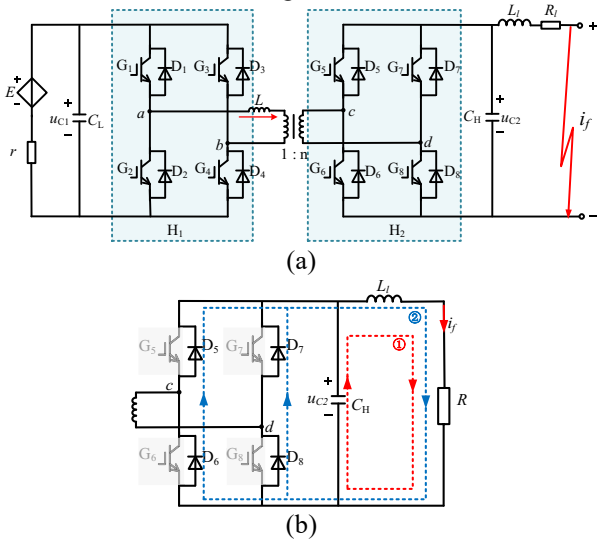

Fig. 8 (a) Schematic diagram of equivalent circuit in structure_3, (b) Fault equivalent circuit of structure_3.

Stage 1: the capacitor discharge stage. C_H discharges towards the fault point through L_l and R_l, causing u_{C2} to gradually decrease. The fault loop is shown in Fig.8(b). The corresponding second-order fault loop equation can be derived based on the circuit structure:

$$L_l C_H \frac{d^2 u_{C2}}{dt^2} + RC_H \frac{du_{C2}}{dt} + u_{C2} = 0 \tag{10}$$

The characteristic roots (λ_1 and λ_2) of the solved equation are (11). In the case where the fault has the greatest impact on the grid, the circuit is in underdamped state, and λ_1 and λ_2 are a pair of complex conjugate roots.

$$\lambda_{1,2} = -\alpha \pm j\beta = -\frac{R}{2L_l} \pm j\sqrt{\frac{1}{L_l C_H} - \frac{R^2}{4L_l^2}} \tag{11}$$

Assuming the fault happen at $t = 0$, $u_{C2}(0) = U_{C2}$, $i_f(0) = 0$, u_{C2} and i_f can be expressed as (12) and (13).

$$u_{C2}(t) = U_{C2} \cdot \frac{\sqrt{\alpha^2 + \beta^2}}{\beta} e^{-\alpha t} \cos(\beta t - \theta) \tag{12}$$

$$i_f = C_H \frac{du_2}{dt} = \frac{U_{C2}}{\beta L_l} e^{-\alpha t} \sin(\beta t) \tag{13}$$

Where $\theta = \arctan(\alpha / \beta)$.

Stage 2: the diode conduction stage. At $t_2 = (\theta + \pi/2)/\beta$, u_{C2} drops to 0. L_l continues to discharge the fault point through the freewheeling diodes D_5~D_8, causing i_f to gradually decrease. The fault loop is shown in Fig.8(b). At this stage, the initial value of i_f is given by (14), and the expression for the fault current can be derived as (15).

$$I_{f2} = i_f(t_2) = \frac{U_{C2}}{L_l\sqrt{\alpha^2 + \beta^2}} e^{-\alpha t_2} \tag{14}$$

$$i_f(t) = I_{f2} e^{-\frac{R}{L_l}(t - t_2)} \tag{15}$$

Once the energy in L_l is fully discharged, the system reaches a steady state, and the fault current in the circuit drops to zero, achieving self-clearing of the fault.

3.2 Simulation verification and result discussion

The above theoretical analysis is verified through simulation using PSCAD/EMTDC. The simulation model of BESS as shown in Fig.9 is constructed, with the DC/DC converter structured as both Buck-Boost and DAB. The parameters used in the simulation are provided in Table 1.

The fault characteristics of the three grid-connected structures in BESS are compared. At t = 0ms, a pole-to-pole fault (fault1) occurs on the DC line connecting to the battery clusters, the fault current is shown in Fig.10. At t = 3ms, the fault current in structure_1 rises to 78.32kA, reaching a near steady-state value of 103.20kA by t = 13ms. In structure_2, the battery clusters also feed into the fault point. At t = 3ms, the fault current rises to 23.34kA, reaching 65.29kA by t = 13ms. The rise rate of fault current within 3ms for structure_1 is approximately 3.36 times that of structure_2, and the time to reach steady-state fault current is approximately 1/4 of the latter. Compared to structure_1, the fault propagation speed is reduced in structure_2 as Buck-Boost converters are installed at the front end of the battery clusters. In structure_3, at t = 0.31ms, the fault current reaches its peak, with the peak value of 9.67kA. At t = 3ms, the fault has entered the diode conduction stage, and the fault current has decayed to 2.47kA, reaching nearly 0 by t = 13ms.

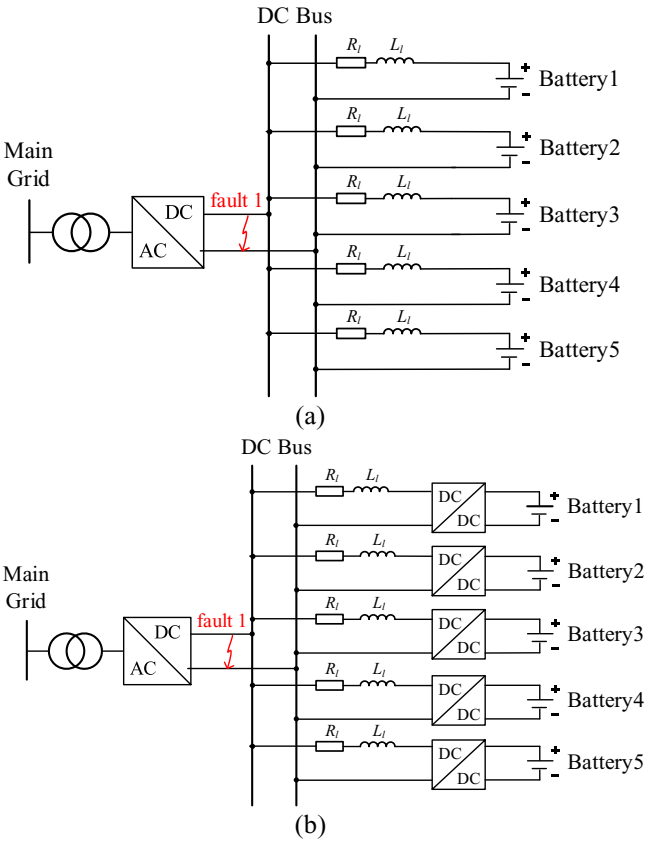

Fig. 9 Schematic Diagram of pole-to-pole fault on DC line. (a) structure_1, (b) structure_2 and structure_3.

Table 1 Simulation Parameters

Parameters		Value
Rated voltage of battery cluster (V)		600
Battery cluster capacity (Ah)		720
The number of battery cluster		5
initial SOC of battery cluster		1
DC bus voltage (V)		750
L_l (μH)		68.275
R_l (mΩ)		28.0
DC/DC output power (kW)		100
Buck-Boost	C_L (μF)	350
	C_H (μF)	100
	L_t (μH)	600
DAB	C_L (μF)	25
	C_H (μF)	600
	L (μH)	25

Based on the simulation verification results, the DC fault interruption requirements for the three grid-connected structures are as follows:

(1) Under structure_1, the fault develops rapidly, and protective devices cannot respond and act in a timely manner. The fault current will cause significant impact and damage to power electronic devices in the grid. The steady-state short-circuit current is too high, exceeding the breaking capacity of existing DC protection devices. Moreover, imbalance between battery clusters can lead to cluster-to-cluster circulation. Therefore, this grid-connected structure should be avoided in BESSs.

(2) Under structure_2, the Buck-Boost converter is a non-isolated DC/DC converter that provides a discharge path for the battery clusters to the fault point. The fault current is the sum of the discharge currents of all battery clusters, and the steady-state fault current exceeds 100kA. From Fig.10(b), it is evident that the faster the operation speed of the protective device, the smaller the current value that needs to be interrupted, indicating a high requirement for the speed and reliability of the protective device.

(3) Under structure_3, the isolated DAB converter achieves electrical isolation, and the fault current is provided solely by the discharge of the DAB high-voltage side capacitors. After the capacitor discharge, the fault current gradually decays to zero, achieving self-clearing of the fault. The difficulty of interrupting the short-circuit fault is significantly reduced, and the requirements for current interruption capability and speediness of protective devices are lowered, which widens the selection range for protective devices.

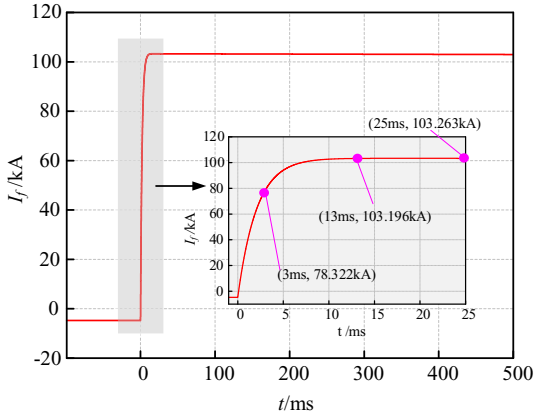

(a)

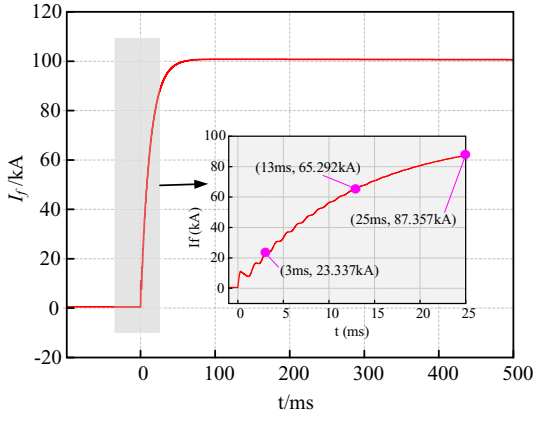

(b)

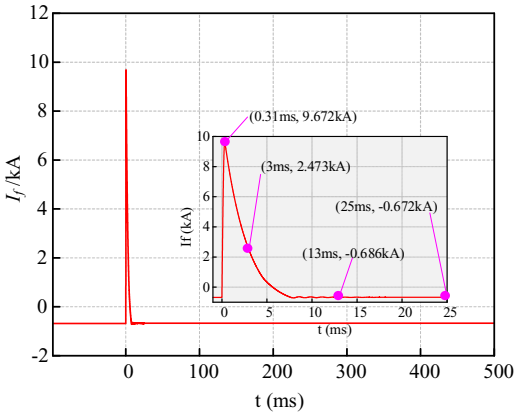

(c)

Fig.10 The fault currents for (a) structure_1, (b) structure_2, (c) structure_3.

4 Comparison

In order to compare the three grid-connected structures, Table 2 provides a comparison of the economic viability, transmission efficiency, and output characteristics of battery clusters for the three grid-connected structures of the simulation model in Section 3.

First, from the economic perspective, the main power electronic devices for the three grid-connected structures are IGBTs and diodes. The three grid-connected structures have the same AC-side structure, so only the structural differences on the DC-side are discussed. Structure_1 has no power electronic devices on the DC-side, while the number of IGBTs in structure_3 is four times that of structure_2. In terms of cost, the cost of structure_2 consists of 10 IGBTs and 5 series inductors of Buck-Boost converters, while the cost of structure_3 consists of 40 IGBTs, 5 inductors and transformers in DABs. Taking the cost of structure_2 as the baseline value of 1p.u., the cost of structure_3 is approximately 3.9p.u..

From the perspective of energy transfer efficiency, only losses in the DC/DC stage are analyzed. The losses of the Buck-Boost converter mainly include device losses and inductor losses, while the losses of the DAB converter mainly include device losses and transformer losses. Compared to device losses, the values of inductor losses and transformer losses are very small and can be neglected. So this paper just focus on device losses. Thermal simulation models for the Buck-Boost and DAB converters are established in PLECS, with a rated power of 100kW for both converters using FF600R17ME4P IGBT modules. The device losses for the Buck-Boost and DAB converters are shown in Table 2, and the device losses of structure_3 are 2.5 times that of structure_2.

From the perspective of addressing inter-cluster circulating current issues, differences in internal parameters of individual batteries and environmental parameters in structure_1 lead to cluster-to-cluster circulating current. However, in structure_2 and structure_3, DC/DC converters are deployed at the output of each battery cluster to regulate

the output voltage of the battery cluster, ensuring its consistency and effectively suppressing cluster-to-cluster circulating current.

Table 2 Comparison of different grid-connected structures

	Structure_1	Structure_2	Structure_3
The number of IGBT	0	10	40
Cost (p.u.)	-	1	3.9
DC/DC power device loss (delivered power set at 100kW)	-	1862.68	6834.70
Whether the inter-cluster circulation current exists	Yes	No	No

In summary, based on the comprehensive comparison, structure_2, while optimizing the output characteristics of the battery clusters, combines economic and efficient features, making it the most suitable grid-connected structure for existing BESSs. According to the analysis of fault interruption requirements, the BESS with structure_2 is suitable for implementing line protection by DC circuit breaker with current-limiting function.

5 Conclusion

Starting from the perspective of grid-connected structures in BESSs, the characteristics of DC line faults and the requirements for fault interruption in BESSs are demonstrated in this paper. Theoretical analysis and verification through PSCAD simulations are conducted for each grid-connected structure under pole-to-pole faults. The comparison shows that as long as DC breaker for BESS could be broken through, structure_2, with advantages of cost-effective and high-efficient, is more suited for existing BESSs.

6 Acknowledgements

This work was supported by Science and Technology Project of the State Grid Cooperation of China (5108-202218280A-2-440-XG).

7 References

[1] M. Liu et al., 'A Review of Power Conversion Systems and Design Schemes of High-Capacity Battery Energy Storage Systems,' in IEEE Access, 2022, 10, pp. 52030-52042.

[2] G. Wang et al., 'A Review of Power Electronics for Grid Connection of Utility-Scale Battery Energy Storage Systems,' in IEEE Transactions on Sustainable Energy, vol. 7, no. 4, pp. 1778-1790, Oct. 2016.

[3] M. Liu et al., 'A Review of Power Conversion Systems and Design Schemes of High-Capacity Battery Energy Storage Systems,' in IEEE Access, 2022, 10, pp. 52030-52042.

[4] M. T. Lawder et al., 'Battery Energy Storage System (BESS) and Battery Management System (BMS) for Grid-Scale Applications,' in Proceedings of the IEEE, vol. 102, no. 6, pp. 1014-1030, June 2014.

[5] K. Zhang, X. Hu, Y. Liu, X. Lin and W. Liu, 'Multi-fault Detection and Isolation for Lithium-Ion Battery Systems,' in IEEE Transactions on Power Electronics, vol. 37, no. 1, pp. 971-989, Jan. 2022.

[6] M. Seo, M. Park, Y. Song and S. W. Kim, 'Online Detection of Soft Internal Short Circuit in Lithium-Ion Batteries at Various Standard Charging Ranges,' in IEEE Access, 2020, 8, pp. 70947-70959.

[7] J. Yang, J. E. Fletcher and J. O'Reilly, 'Short-Circuit and Ground Fault Analyses and Location in VSC-Based DC Network Cables,' in IEEE Transactions on Industrial Electronics, vol. 59, no. 10, pp. 3827-3837, Oct. 2012.

[8] Z. Zhang, Q. Chen, R. Xie and K. Sun, 'The Fault Analysis of PV Cable Fault in DC Microgrids,' in IEEE Transactions on Energy Conversion, vol. 34, no. 1, pp. 486-496, March 2019.